PAGEOPH, Vol. 147, No. 4 (1996)

0033–4553/96/040611–19$1.50 + 0.20/0

Modelling Shear Waves in OBS Data from the Vøring Basin (Northern Norway) by 2-D Ray-tracing

P. DIGRANES,[1] R. MJELDE,[1] S. KODAIRA,[2] H. SHIMAMURA,[2] T. KANAZAWA,[3] H. SHIOBARA,[3] and E. W. BERG[4]

Abstract—Three component recordings from an array of five ocean bottom seismographs in the northwestern part of the Vøring basin have been used to obtain a 2-D shear-wave (*S*-wave) velocity-depth model. The shear waves are identified by means of travel-time differences compared to the compressional (*P*) waves, and by analyzing their particle motions. The model has been obtained by kinematic (travel-time) ray-tracing modelling of the OBS horizontal components.

The shear-wave modelling indicates that mode conversions occur at several high velocity interfaces (sills) in the 4–10 km depth range, previously defined by a compressional-wave velocity-depth model using the same data set.

An average V_p/V_s ratio of 2.1 is inferred for the layers above the uppermost sill, indicative of both poorly consolidated sediments and a low sand/shale ratio. A significant decrease in the V_p/V_s ratio (1.7) below the first sill may in part be attributed to well consolidated sediments, and to a change in lithology to more sandy sediments. This layer is interpreted to lie within the lower Cretaceous sequence. At 5–10 km depth V_p/V_s ratios of 1.85 indicate a lower sand/shale ratio consistent with the expected lithologies. The average V_p/V_s ratio inferred for the crust is 1.75, which is consistent with values obtained north of Vøring, in the Lofoten area. An eastward thinning of the crystalline basement is supported by the shear-wave modelling.

Key words: Vøring basin, 3C OBS data, shear waves.

Introduction

In 1992 an extensive seismic experiment using three-component Ocean Bottom Seismographs (OBS) was conducted on the Vøring margin (Figure 1) from R/V Håkon Mosby, University of Bergen (MJELDE *et al.*, 1996). Scientists from the Universities of Bergen, Hokkaido and Tokyo as well as Statoil participated in the acquisition. The objective was to map the regional crustal structures in the Vøring Basin, and to evaluate contributions from the ocean bottom seismometer (OBS) method as an aid in hydrocarbon prospecting.

[1] Institute of Solid Earth Physics, University of Bergen, Allegt. 41, 5007 Bergen, Norway.
[2] Laboratory for Ocean Bottom Seismology, Hokkaido University, Sapporo 060, Japan.
[3] Earthquake Research Institute, Tokyo University, Yayoi 1-1-1 Bunkyo-ku, Tokyo 113, Japan.
[4] Statoil R&D, Postuttak, 7004 Trondheim, Norway.

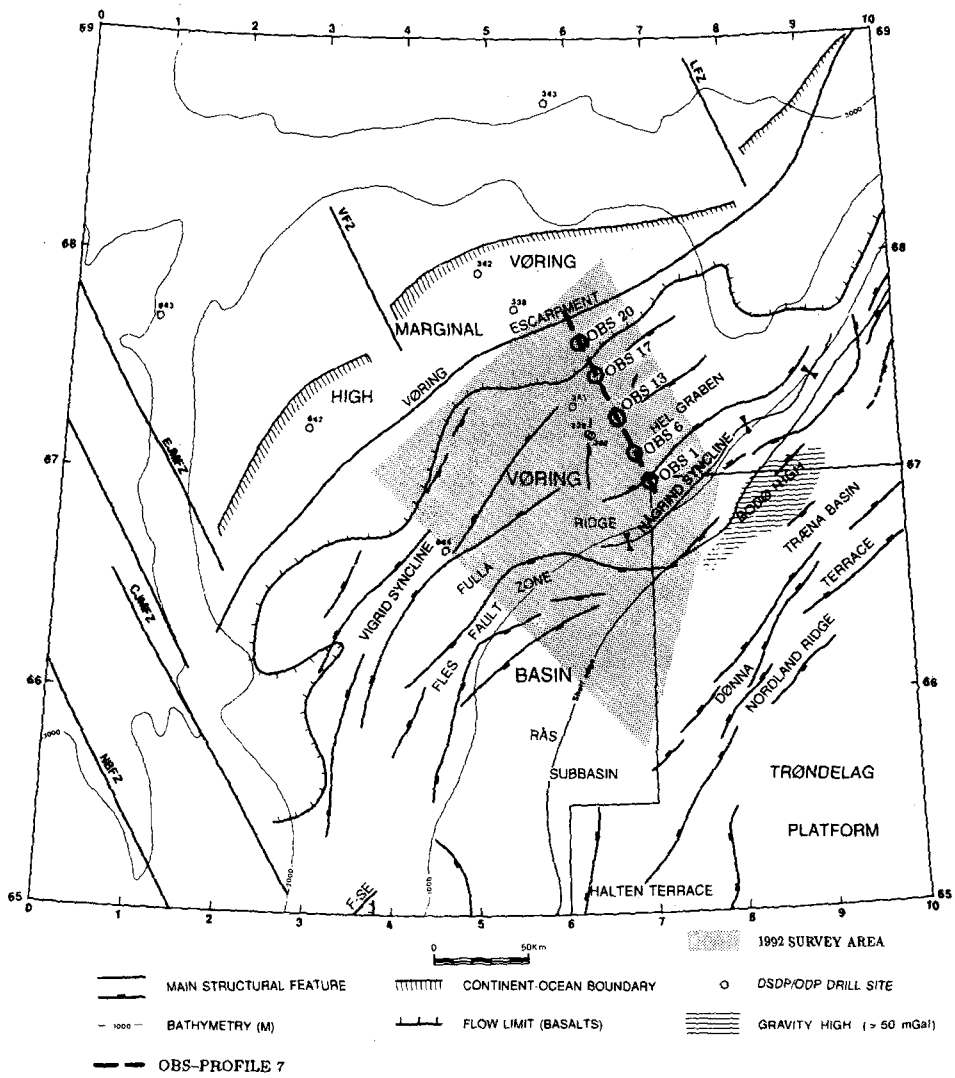

Figure 1
Map showing the 1992 OBS survey area, and the main structural features in the Vøring basin and adjacent areas. Position of OBS profile 7 and modelled OBSs are indicated. F-SE = Faeroe-Shetland Escarpment; NBFZ = Norway Basin fracture zone; CJMFZ = central Jan Mayen fracture zone; EJMFZ = East Jan Mayen fracture zone; LFZ = Lofoten fracture zone; VFZ = Vøring fracture zone. Modified after SKOGSEID *et al.* (1992).

A seismic compressional-wave model, based on modelling of five OBS instruments along one profile, was presented by MJELDE *et al.* (1996). In this study we describe modelling of the horizontal components for the same five OBS instruments, in order to establish the conversion depths and velocities for the observed shear waves.

Geological Framework

The Vøring margin has been investigated for more than two decades, from acquisition and interpretation of multichannel seismic reflection data (BØEN *et al.*, 1984; SKOGSEID and ELDHOLM, 1989), seismic refraction data (ELDHOLM and MUTTER, 1986), commercial drilling on the continental shelf (SPENCER, 1984, 1986; DALLAND and WORSLEY, 1988) and scientific drilling at the Vøring Plateau (TALWANI *et al.*, 1976; ELDHOLM *et al.*, 1987, 1989).

A number of extensional episodes have been documented along the margin since Devonian time: late Carboniferous-early Permian regional rifting, mid to late Triassic block faulting and late Triassic-early Jurassic growth faulting with detachment in Triassic evaporites (LARSEN *et al.*, 1989; SURLYK *et al.*, 1984). A minimum of 3 km of pre-Cretaceous sediments is inferred regionally in the Vøring Basin (BØEN *et al.*, 1984; SKOGSEID and ELDHOLM, 1989), while as much as 10 km may exist locally (ELDHOLM and MUTTER, 1986; PLANKE *et al.*, 1991). The late Jurassic-early Cretaceous extension led to major faulting, with reactivation of older fault zones, and generation of slightly rotated fault blocks which subsequently subsided along the major rift systems (BØEN *et al.*, 1984; HINZ *et al.*, 1984; MUTTER, 1984; RØNNEVIK *et al.*, 1983; SKOGSEID and ELDHOLM, 1989). The maximum early Cenozoic extension axis shifted westward with respect to the Jurassic-Cretaceous tectonic episode. The late Cretaceous-early Cenozoic extension episode lasted for as much as 18–20 Myr and finally caused continental separation in the earliest Eocene. During the syn-rift phase the outer Vøring Basin was uplifted, and an area about 120 km wide was exposed to erosion. The landward limit of a marginal high (the Vøring Escarpment) is presently observed below $\approx$2 km of post opening sediments. The late syn-rift period was associated with high magmatic activity, which caused accretion of thick magmatic bodies at the base of the crust, emplacement of sills in the adjacent Cretaceous sediments and extrusive volcanism forming large wedges of flood basalt (ELDHOLM *et al.*, 1989).

Mode Conversion

Using air-guns fired in the water layer, the observed shear waves must be generated by mode conversion at different subsurface interfaces. Mode conversion occurs when a compressional wave encounters an interface at non-normal angles of incidence. The total amount of compressional-wave energy converted into both reflected and transmitted shear waves can be described by the Zoeppritz equations (SCHOENBERG and PROTÁZIO, 1992). As the compressional-wave angle of incidence increases, the amplitudes of the transmitted shear waves increase, and at angles of incidence beyond the compressional-wave critical angle, mode conversion might be quite significant. In Figure 2 the theoretical partitioning of energy between the

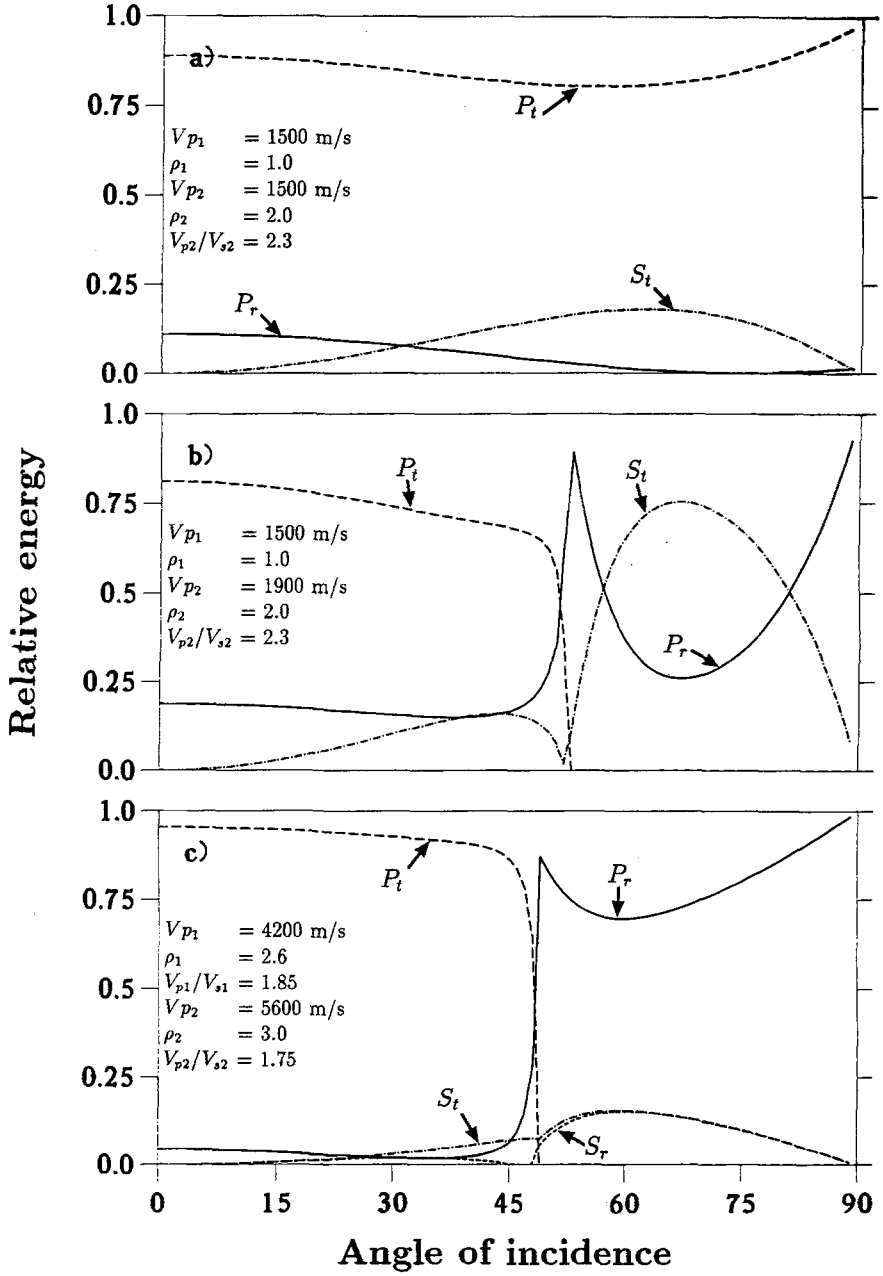

Figure 2

Theoretical partitioning of energy from a P-wave incident at the seafloor (2a, 2b), and at a sediment/sill interface (2c) (sediment/sill interface 9 in Fig. 8). Velocities, densities and V_p/V_s ratios are indicated in the figure. P_r, P_t, S_r and S_t refer to reflected P energy, transmitted P energy, reflected S energy and transmitted S energy, respectively.

different wave modes is illustrated for three different cases. The compressional- and shear-wave velocities used are inferred from the modelling of profile 7. In Figure 2a the seafloor compressional-wave velocity is 1500 m/s, and the main part of the incident energy is transmitted as compressional-wave energy. At angles of incidence between 45°C and 75° more than 15% of the energy is transmitted as mode converted shear waves. A higher seafloor velocity (Fig. 2b) results in a more efficient mode conversion. At angles of incidence beyond the compressional-wave critical angle approximatley 50% of the energy is transmitted as mode converted shear waves. Figure 2c illustrates the theoretical response at a sediment/sill interface. At a depth of ≈ 6 km the velocity contrast is relatively low, and at angles of incidence below the compressional-wave critical angle more than 90% of the energy is transmitted as compressional-wave energy. From 25° to 40° the amount of energy reflected as compressional- and shear-waves is equal. At angles of incidence beyond the compressional-wave critical angle as much as 20% of the incident energy is converted into reflected/transmitted shear waves.

In an isotropic, horizontally layered model the particle motion of the mode converted shear wave will be entirely in the vertical plane. In a more realistic model, the particle motion depends on layer dip and degree of anisotropy. The OBS data is recorded on three component gimballed geophones, hence the different wave modes can be identified based on their particle motions.

Data Processing

The 3-component OBS data have been a/d converted at the University of Hokkaido, Japan, and the processing has been performed at the Institute of Solid Earth Physics (IFJ), University of Bergen.

An example of the raw data is shown in Figure 3. The data were contaminated by low frequent noise, and several bandpass filters were tested in order to attenuate the noise without distorting the signal. The low-frequency/high gain OBS data seem to be robust, in the sense that small changes in the filter parameters do not visually affect the data. The 5–12 Hz bandpass filter used on the vertical components gave a good result on the horizontal components as well (Fig. 4), and the following testing was performed with this filter.

The bandpass filtered data (Fig. 4) have a "ringy" appearance, and deconvolution filters were tested to attenuate the "ringing". A predictive deconvolution with a 32 ms gap, 250 ms operator length and 3000 ms design window gave a good result (Figs. 5 and 6). The same deconvolution filter was applied on the horizontal and vertical components, the only difference being the start time of the design window. This was chosen so as to include the main compressional- and shear-wave events on the vertical and horizontal components, respectively.

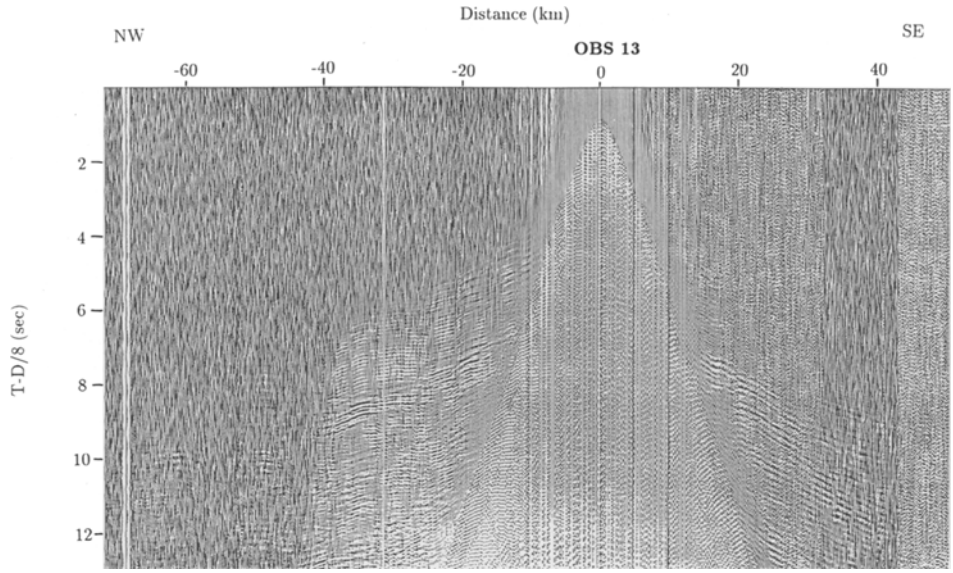

Figure 3
Horizontal high-gain component of OBS 13, no processing applied. Notice low-frequent noise. Reduction velocity 8.0 km/s.

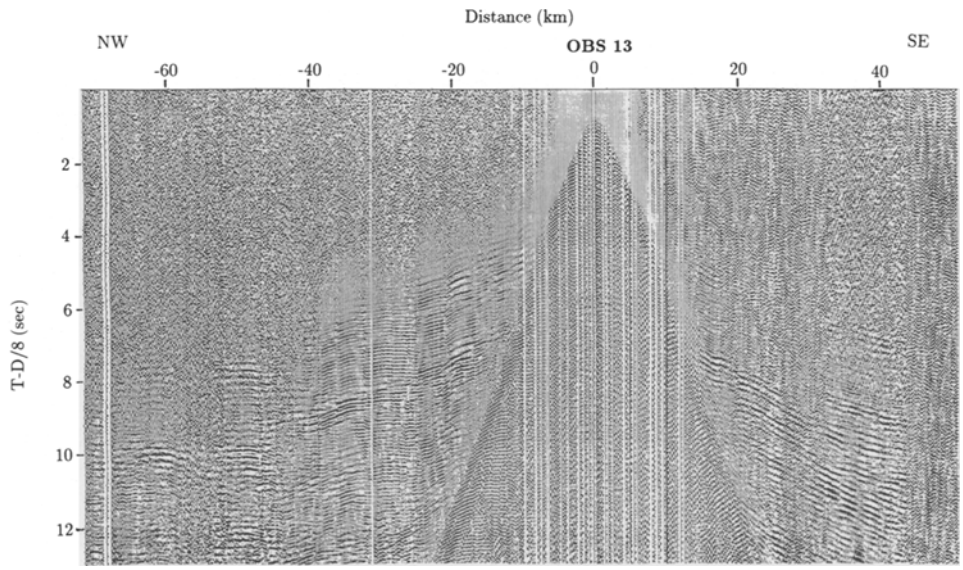

Figure 4
Horizontal high-gain component of OBS 13, 5–12 Hz bandpass filter applied. Reduction velocity 8.0 km/s.

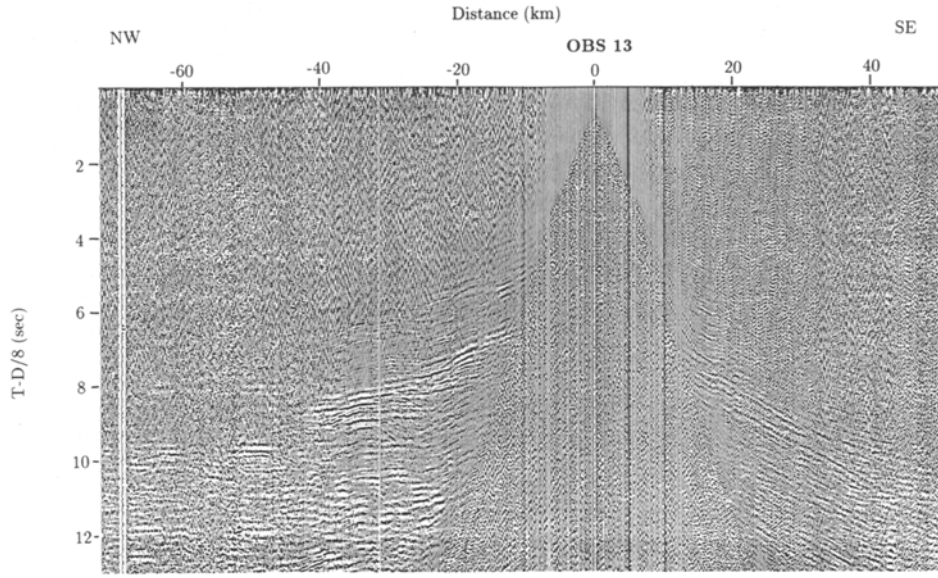

Figure 5
Horizontal high-gain component of OBS 13, 5–12 Hz bandpass filter and deconvolution applied. Reduction velocity 8.0 km/s.

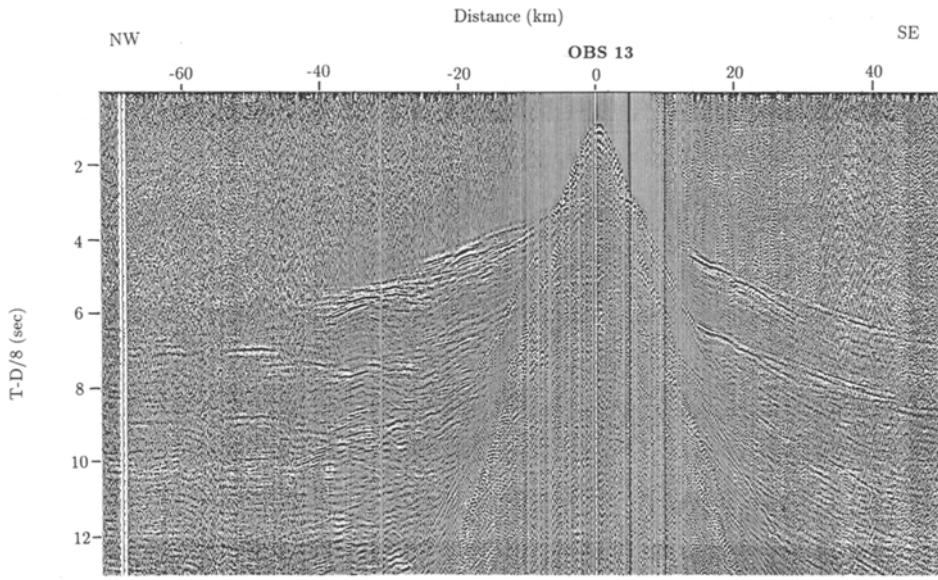

Figure 6
Vertical high-gain component of OBS 13, 5–12 Hz bandpass filter and deconvolution applied. Reduction velocity 8.0 km/s.

In order to enhance the quality of the shear waves on the horizontal components velocity filtering was tested. This did not improve the data quality, probably due to aliasing effects caused by the coarse spatial sampling (240 m shot point distance).

Identification of Shear-wave Arrivals

In order to identify the shear-wave arrivals an interpretation of both the horizontal and vertical components was carried out. The H_1 component from OBS 13 is shown in Figure 5 and the vertical component in Figure 6. A key feature in the data is that the vertical and the horizontal components reveal a similar reflection/refraction pattern (Fig. 7). The later arrival times on the horizontal components indicate that these waves mainly represent refracted compressional waves, having travelled partly as shear waves, or P-to-S wide angle reflections. As the compressional and shear waves are orthogonally polarized, plots of the particle motions (hodograms) around the first onset of the shear-wave arrivals are utilized to verify the identification of these phases. In Figure 7 hodograms of the marked events indicate typical particle motions for compressional and shear waves. Additional hodograms are shown in Figure 10.

The quality of the horizontal components varies along the profile, and the number of shallow shear-wave arrivals increases north-westwards. This might be explained by the fact that the number of sills increases towards NW (Fig. 8), since mode-conversions are more likely to occur at these high-velocity interfaces.

Modelling

The OBS data have been modelled using 2-D kinematic (travel-time) ray-tracing to match the first onset of the shear-wave arrivals in order to obtain shear-wave velocities and conversion depths, assuming the P-wave model of MJELDE *et al.* (1996) (Fig. 8). The maximum misfit between the observed and calculated travel times is kept below 200 ms, as for the P-wave modelling of the profile (MJELDE *et al.*, 1996). The bandpass filtered and deconvolved data from OBS 17, as well as the data with calculated travel-time curves superimposed are presented in Figures 10 and 11. The uncertainty in the compressional- and shear-wave velocities is estimated to be $\pm 0.1\ \mathrm{km\ s^{-1}}$, and in the V_p/V_s ratio to be 0.05 (MJELDE and SELLEVOLL, 1993).

The thickness of the sills cannot be determined from the kinematic modelling using constant velocity layers. However, this might be possible by incorporating velocity gradients and performing a dynamic modelling of both the compressional and shear waves reflected/refracted from the sills.

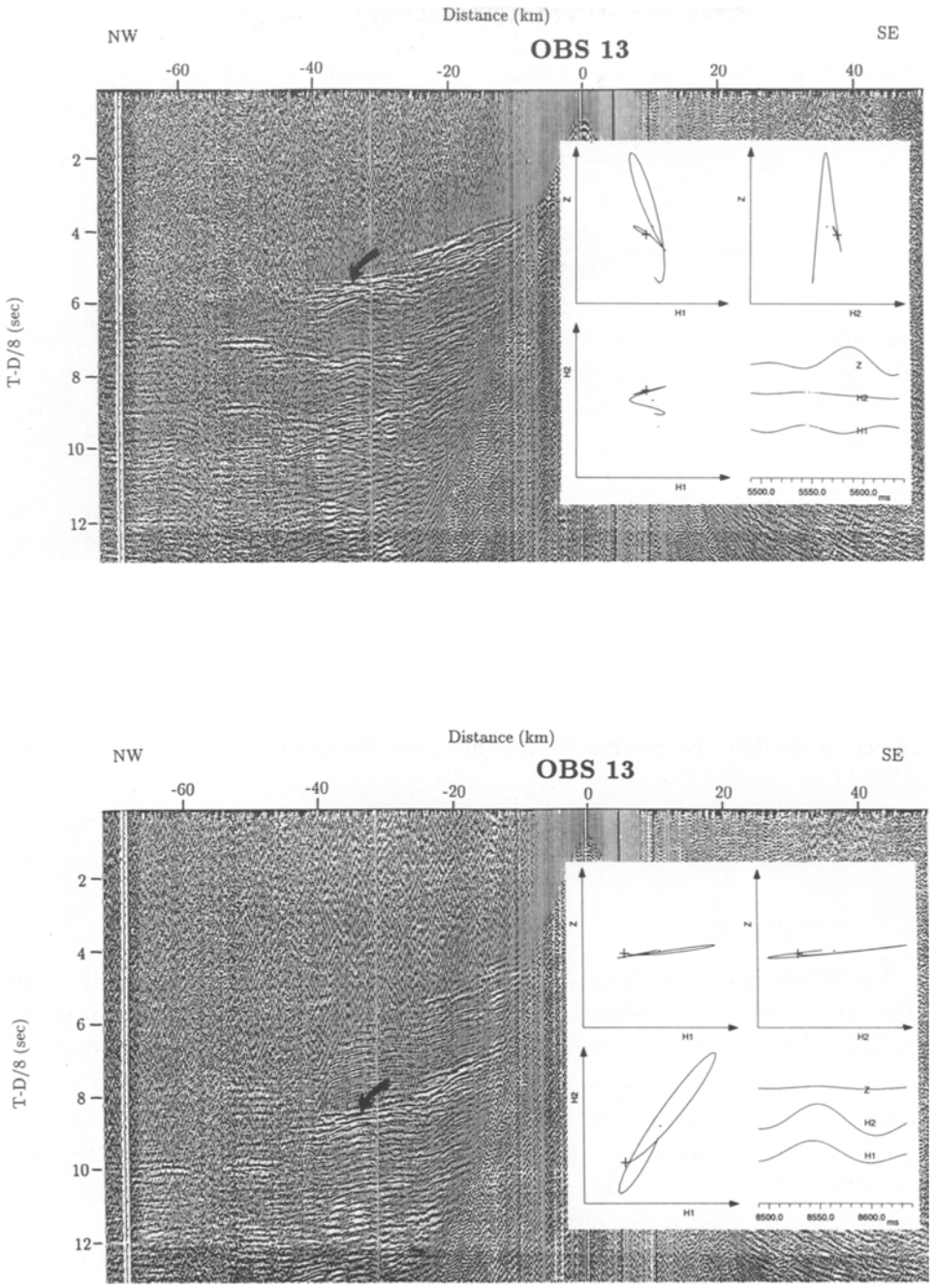

Figure 7

Vertical (upper) and horizontal (lower) high-gain component of OBS 13, 5–12 Hz bandpass filter and deconvolution applied. Reduction velocity 8.0 km/s. Polarization plot of arrival indicated with arrow shown on the right-hand side of the figure. Note the main particle motion in the vertical (upper) and horizontal (lower) plane, indicating a *P* and *S* wave, respectively.

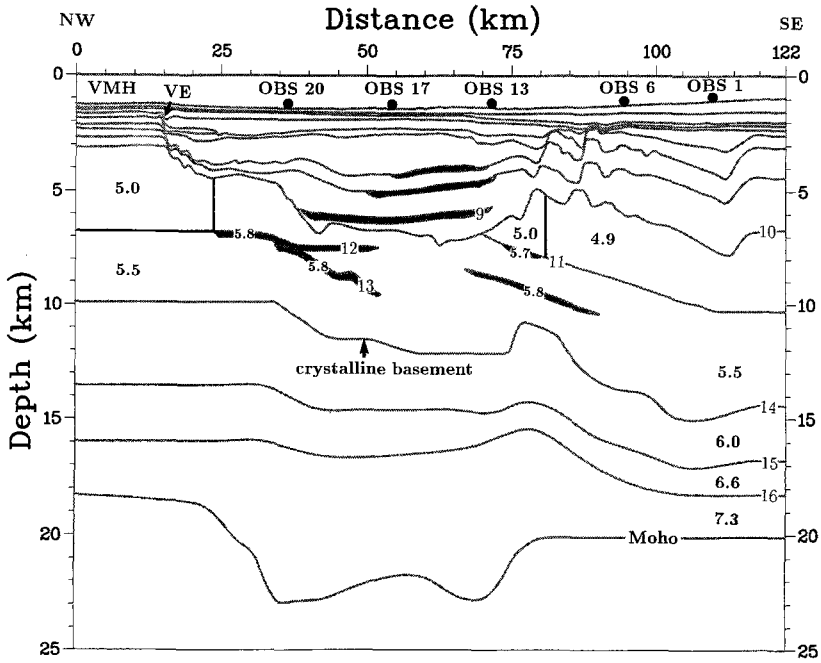

Figure 8
The 2-D regional model of the OBS profile, with seismic *P*-wave velocities (in km/s) for the deep part indicated. VMH = Vøring Marginal High; VE = Vøring Plateau Escarpment.

Discussion

V_p/V_s and Lithology

The relationship between V_p/V_s and lithology is well established both from laboratory experiments and case studies (PICETT, 1963; DOMENICO, 1984; GAROTTA, 1985; TATHAM, 1985; TATHAM and MCCORMAC, 1991). Variations in other

Table 1

Ranges of V_p/V_s values in typical sedimentary rocks. (After DOMENICO, 1984)

Rock	V_p/V_s
Sandstone	1.59–1.76
Calcareous Sandstone	1.67–1.76
Dolomite	1.78–1.84
Limestone	1.84–1.99
Shale	1.7–3.00

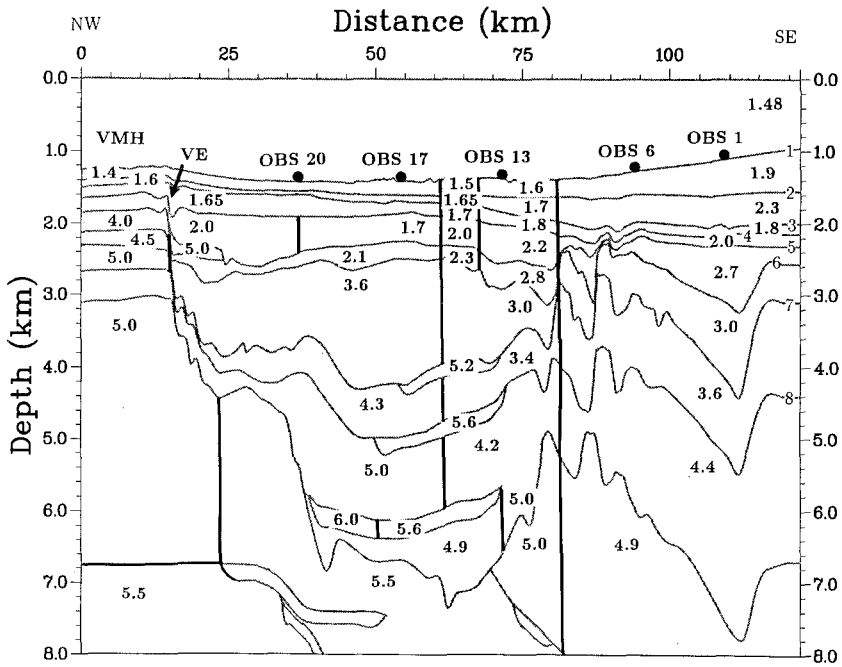

Figure 9
The 2-D regional model of the OBS profile, with seismic P velocities for the shallow part indicated. VMH = Vøring Marginal High; VE = Vøring Plateau Escarpment.

rock properties like porosity and pore fluid also affect the elastic wave velocities, hence the V_p/V_s ratio is not unique as a lithological indicator. Therefore, available geological and geophysical information should be considered in order to optimize a lithologic interpretation.

DOMENICO (1984) used laboratory measurements to compute V_p/V_s ranges for common sedimentary lithologies and his results are summarized in Table 1. The low end of the range is associated with sandstones, and the high end with carbonates and shales. With the exception of the velocity ratio range for shale, the V_p/V_s intervals represent 90% confidence intervals. There are not enough reliable shale measurements to provide a statistical confidence interval at present (TATHAM and MCCORMAC, 1991).

Modelling Results

In this section the modelled interfaces and S velocities will be described, using the numeration indicated in Figures 8 and 9. The layers are numbered according to the interface below; layer 1 being the water layer, etc. Figures 12 and 13 show the shear-wave velocity model with the V_p/V_s ratios indicated. Mode conversions are

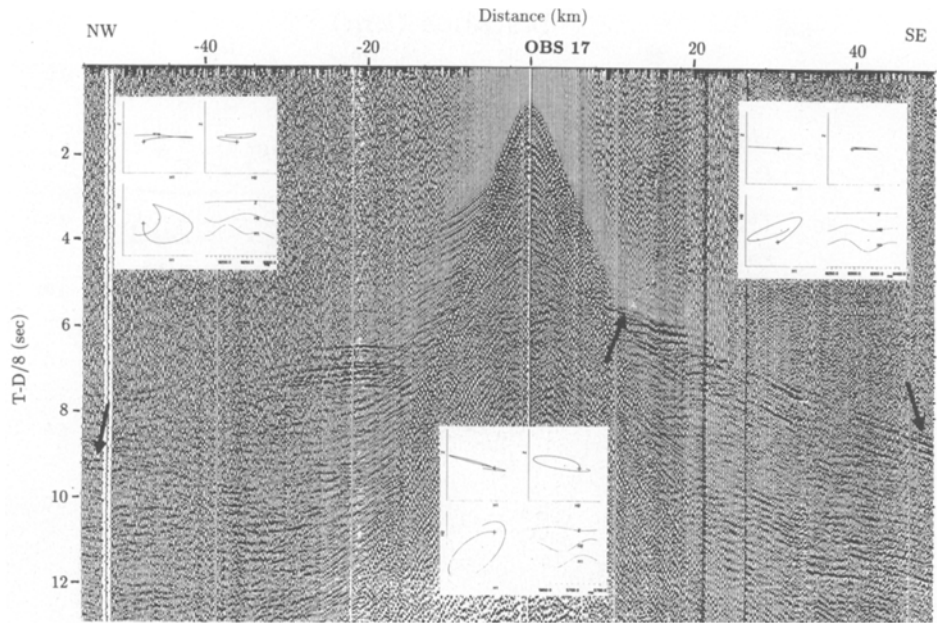

Figure 10
Horizontal high-gain component of OBS 17, 5–12 Hz bandpass filter and deconvolution applied. Reduction velocity 8.0 km/s. The particle motion of the marked events is shown in the figure.

modelled to occur primarily at the interfaces where the shear waves are reflected/refracted, and at the seafloor in the eastern part of the profile. In particular, the high velocity sill intrusions act as effective conversion interfaces. The 2-D *P*-wave model with marked conversion interfaces is shown in Figure 12.

The uppermost horizon mapped by the shear waves is interface 7 (Fig. 13), hence only the average V_p/V_s ratio in layers 2–7 can be inferred. A detailed lithological interpretation is thus not possible in this interval. Low seafloor velocities (Fig. 9) and a relatively high average V_p/V_s ratio of 2.1 in layers 2–7 indicate poorly consolidated sediments in the upper layers.

Interfaces 7 and 8 are both mapped by the shear waves, and the V_p/V_s ratio in layer 8 is inferred to be 1.70. This is a significantly lower value compared to the interval above, and may in part be attributed to well consolidated sediments, and to a change in lithology to more sandy sediments.

Interface 9 coincides locally with the third uppermost sill, and a refracted *S* arrival in OBS 20 indicates a V_p/V_s ratio of 1.75 in the sill. This corresponds well with values obtained from ODP drillhole 642 (Fig. 1) on the outer Vøring margin (BARTON *et al.*, 1989). The V_p/V_s ratio in layer 10 is inferred to be 1.85, which is higher than in the layer above. This may be interpreted as a decrease in the sand/shale ratio in these sediments compared with layer 8.

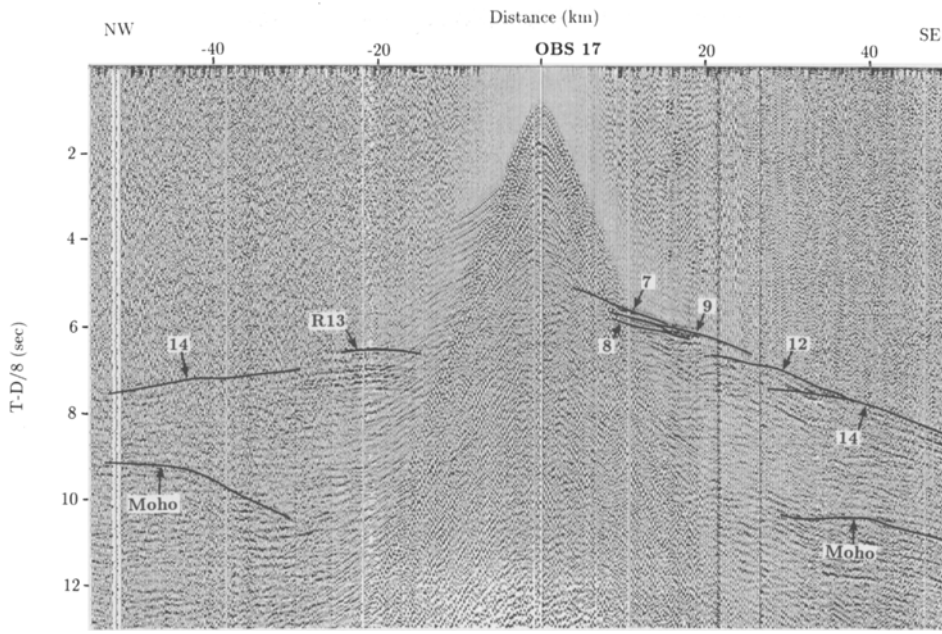

Figure 11
Horizontal high-gain component of OBS 17, 5–12 Hz bandpass filter and deconvolution applied. Reduction velocity 8.0 km/s. The indicated arrivals refer to travel-time curves calculated by ray-tracing from the model in Figure 8. Arrivals marked with *R* represent reflections, other arrivals correspond to critical refractions. Numbers correspond to interfaces in the *P*-wave model (Fig. 8).

Interfaces 12 and 13 are interpreted to represent sills intruded into the deepest sedimentary layer (MJELDE *et al.*, 1996). Modelling of shear-wave arrivals from these sill intrusions indicates a V_p/V_s ratio of 1.85 in layer 14. Interface 14 is interpreted to represent the top of the crystalline basement due to the relatively good lateral continuity and the high *P*-wave velocity below (6 km/s) (MJELDE *et al.*, 1996). The crystalline basement is clearly mapped by the shear waves, and modelling of these arrivals confirms the V_p/V_s ratio of 1.85 in layer 14. This may indicate a low sand/shale ratio in the pre-Cretaceous sediments.

Interface 17 is interpreted to represent the Moho (base of the crust) (MJELDE *et al.*, 1996). Both wide-angle reflections and refractions are observed from the Moho, but interfaces 15 and 16 are not observed as shear-wave arrivals. Consequently only the average V_p/V_s ratio below the crystalline basement can be inferred through the modelling. The average V_p/V_s ratio obtained is 1.75, which is consistent with values obtained further north, in the Lofoten area (MJELDE and SELLEVOLL, 1993).

Geological Implications

The OBS profile is located in the northwestern part of the Vøring basin (Fig. 1) where presently well control is limited to the Neogene section. The modelling of the

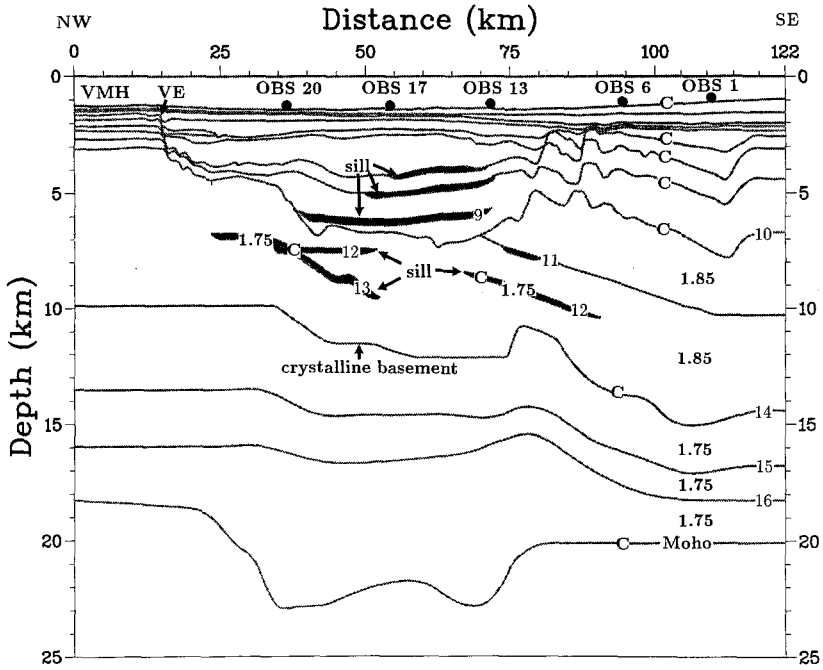

Figure 12
The 2-D regional model of the OBS profile, with V_p/V_s ratios for the deep part indicated. Conversion interface indicated with a 'C'. VMH = Vøring Marginal High; VE = Vøring Plateau Escarpment.

horizontal components along the OBS profile provides the average V_p/V_s ratio in layers 2–7 (2.10), layer 8 (1.70), layer 10 (1.85), layer 14 (1.85) and layers 15–17 (1.75) (Figs. 12 and 13). The V_p/V_s ratio can be interpreted in terms of changes in lithology, as discussed earlier in this section. The low average V_p/V_s ratio inferred for the uppermost layers (layers 2–7) is related to poorly consolidated sediments, which is consistent with the low compressional-wave velocities in the shallow sediments. The significantly lower V_p/V_s ratio in layer 8 (1.70, Fig. 13) might indicate more sandy sediments at this level; at 4–5 km depth in the central graben and at 3.5–5 km depth in the eastern syncline. Layer 8 occurs within the lower Cretaceous sequence according to the interpretation of the base Cretaceous horizon in this area (SKOGSEID and ELDHOLM, 1989; SKOGSEID *et al.*, 1992; SKOGSEID pers. comm., 1994).

The history of subsidence and uplift in the Vøring Basin area has been discussed by BØEN *et al.* (1984), HINZ *et al.* (1984), MUTTER (1984), SKOGSEID and ELDHOLM (1989), SKOGSEID *et al.* (1992), among others. Seismic stratigraphic interpretations suggest basin subsidence during the Cretaceous period. SKOGSEID and ELDHOLM (1989) interpret the absence of regionally continuous reflectors within the Cretaceous sequence as indicative of homogenous sediments, probably a

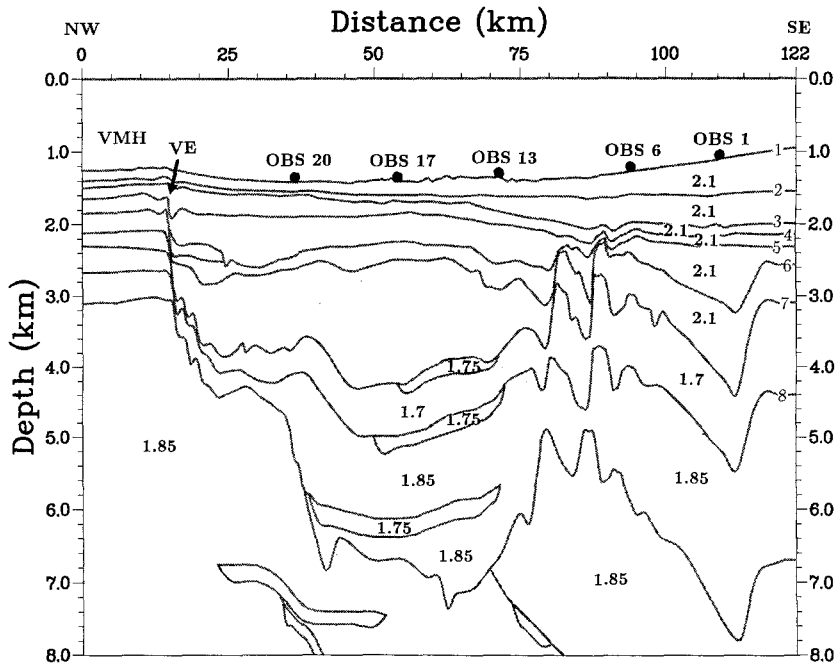

Figure 13
The 2-D regional model of the OBS profile, with V_p/V_s ratios for the shallow part indicated. The dotted part of the Moho from PLANKE *et al.* (1991). VMH = Vøring Marginal High; VE = Vøring Plateau Escarpment.

considerable component of marine shales. However, within the western rifts they observe an increase in internal reflectivity that might reflect coarser sediment components, possibly derived from erosion of the adjacent highs. SKOGSEID *et al.* (1992) pointed out that sand bodies may exist along both sides of the Fulla ridge and locally along the Bodø High. These highs experienced local rift related uplift during the early Cretaceous and were thus prone to erosion. They further suggest that these sand bodies may be genetically correlated with the Cenomanian and Turonian sand-prone deposits drilled west of the Nordland Ridge (HASTINGS, 1986). The V_p/V_s ratio inferred for layer 8 in our model supports the existence of local sand layers in the lower Cretaceous. One should note that the horizons defining layer 8 are traced continuously over the rotated fault blocks (below OBS 13–6, Fig. 13). However, a cautious approach is necessary both when interpreting the reflection seismic data across fault blocks and when correlating with the geological model.

The V_p/V_s ratio inferred for layers 10 and 14 (1.85), indicates a change in lithology as compared to layer 8. We infer layers 10 and 14 (Fig. 12) to be sediments of pre-Cretaceous and possibly earliest Cretaceous age. The pre-Cretaceous sedimentary layers are less well resolved both in the seismic data (SKOGSEID

et al., 1992) and in our model. Consequently the V_p/V_s ratios obtained for layers 9/10 and 14 reflect the average V_p/V_s ratio for the different sedimentary units within these layers. The expected main lithological units are: late Permian carbonates, clastic sediments of Triassic age, predominance of sandstones in the Jurassic and earliest Cretaceous marine shales (DORÉ, 1991; LARSEN, 1987; SKOGSEID *et al.*, 1992). This yields a shale/sand lithology in layers 9/10, and a sand/clastics/carbonate lithology in layer 14, consistent with the inferred V_p/V_s ratios. It should be emphasized that a more detailed lithological interpretation of these layers would be speculative due to the uncertainties in both the seismic interpretation and the model. The average V_p/V_s ratio inferred for layers 15–17 (1.75) (crystalline basement) compares well with values obtained for the crystalline basement further north in the Lofoten area (MJELDE and SELLEVOLL, 1993). It also confirms that the crust is of continental origin in this area (MJELDE and SELLEVOLL, 1993; SKOGSEID *et al.*, 1992).

Our model is not well constrained in the westernmost part of the profile, as the OBS in this region is located 20 km east of the Vøring escarpment. An eastward thinning of the crystalline basement to about 5 km thickness (Fig. 12) is required from modelling the horizontal components. SKOGSEID (pers. comm., 1994) inferred a minimum thickness of 7 km of the crystalline crust in this area from studies of ESP and sonobuoy data. This thinning is explained as the result of several rift episodes. From the relative thicknesses of the pre-Cretaceous (below layer 8, Figs. 12 and 13), the Cretaceous and later sediments it is evident that the main extension was centered in the eastern part of the Vøring basin in pre-Cretaceous time. The early Cenozoic extension occurred in the western Vøring basin and lead to the breakup and continental separation between Norway and Greenland in the early Eocene. The level of the base Cretaceous reflector is a matter of dispute (BLYSTAD *et al.*, 1995), and the apparent subsidence of the post-Cretaceous sediments in the eastern part of the profile can partly be contributed to compaction of the underlying sediments (SKOGSEID *et al.*, 1992).

Conclusions

A 2-D shear-wave velocity model along the OBS profile in the Vøring basin has been obtained by ray-tracing modelling of the horizontal components of five OBS instruments. The shear waves recorded on the horizontal components are identified by means of travel-time differences compared to the compressional waves and by analyzing their particle motions.

The shear-wave modelling is based on the model geometry and compressional-wave velocities obtained by ray-tracing modelling of the vertical-components along the same profile (MJELDE *et al.*, 1995). The two parameters determined through the shear-wave modelling are shear-wave velocities (i.e., V_p/V_s ratios) in the different layers and conversion depths.

The two-dimensional compressional-wave velocity modelling has mapped sills intruded into the sediments at 4–10 km depth. The shear-wave modelling indicates that mode conversions occur primarily at these high velocity interfaces. The number of sills, as well as shallow S arrivals, increases westwards.

The shear-wave modelling provides the vertical variation in the V_p/V_s ratio, which can be interpreted in terms of changes in the lithology. Interface 7 (the uppermost sill) at 4.0 km depth is the shallowest interface mapped by the modelling. An average V_p/V_s ratio of 2.1 is inferred for the layers above, which is indicative of both a high shale content and/or poorly consolidated sediments. In layer 8, a V_p/V_s ratio of 1.7 is inferred, implying a high sand/shale ratio. According to the interpretation of the base Cretaceous horizon in this area, we interpret this layer to lie within the lower Cretaceous sequence. In layers 9/10 and 14 a V_p/V_s ratio of 1.85 indicates a change in lithology compared to layer 8. This is consistent with the expected shale/sand (layers 9/10) and sand/clastics/carbonate (layer 14) lithology. One S refraction is observed in OBS 20, indicating a V_p/V_s ratio of 1.75 in the sills.

Both the crystalline basement (interface 14) and the Moho are mapped by the shear waves. Interfaces 15 and 16 are not observed on the horizontal components, hence only the average V_p/V_s ratio in the layers below the crystalline basement can be inferred. The modelling indicates an average V_p/V_s ratio of 1.75 in the layers between the crystalline basement and the Moho. This is consistent with values obtained in the Lofoten area further north and confirms that the crust is of continental origin in this area. An eastward thinning of the crystalline basement is required by the shear-wave modelling. From the relative thicknesses of the pre-Cretaceous, the Cretaceous and later sediments it is evident that the main extension episodes were centered in the eastern part of the Vøring basin in pre-Cretaceous time.

Acknowledgements

Professor M. A. Sellevoll at IFJ is greatly acknowledged for his support during the planning of the experiment and comments on the manuscript. We wish to acknowledge Profs. Y. Kristoffersen and J. Skogseid for helpful discussions during the preparations of the manuscript.

Finally, Statoil is thanked for economical support, and for allowing the results to be published.

REFERENCES

BARTON, C., MOOS, D., and BLANGY, J.-P., *Analysis of full waveform acoustic logging data at ODP site 642-outer Vøring Plateau.* In *Proc. ODP, Sci. Res. 104* (College Station, TX 1989) (Ocean Drilling Program) pp. 953–964.

BLYSTAD, P., BREKKE, H., FÆRSETH, R. B., LARSEN, B. T., SKOGSEID, J., and TØRUDBAKKEN, B. (1995), *Structural Elements of the Norwegian Continental Shelf. Part 2: The Norwegian Sea Region*, NPB Bull *8* (Norwegian Petroleum Directorate).

BØEN, F., EGGEN, S., and VOLLETH, J., *Structures and basins of the margin from 62–69°N and their development.* In *Petroleum Geology of the North European Margin* (ed. A. M. Spencer *et al.*) (Graham and Trotman, London 1984) pp. 3–28.

DALLAND, A., and WORSLEY, D. (1988), *A Lithostratigraphic Scheme for the Mesozoic and Cenozoic Succession Offshore Norway North of 62°N*, NPD Bull. *4* (Norwegian Petroleum Directorate).

DOMENICO, S. N. (1984), *Rock Lithology and Porosity Determination from Shear- and Compressional-wave Velocity*, Geophys. *49*, 1188–1195.

DORÉ, A. G. (1991), *The Structural Foundation and Evolution of Mesozoic Sea-ways between Europe and the Arctic*, Pal. *87*, 441–492.

ELDHOLM, O., and MUTTER, J. C. (1986), *Basin Structure of the Norwegian Margin from Analysis of Digitally Recorded Sonobuoys*, J. Geophys. Res. *91*, 3763–3783.

ELDHOLM, O., THIEDE, J., and TAYLOR, E., *Evolution of the Norwegian continental margin: Background and objectives.* In *Proc. ODP, Init, Repts. 104* (College Station, TX 1987) (Ocean Drilling Program) pp. 5–25.

ELDHOLM, O., THIEDE, J., and TAYLOR, E., *Evolution of the Vøring volcanic margin.* In *Proc. ODP, Sci. Res. 104* (College Station, TX 1989) (Ocean Drilling Program) pp. 1033–1065.

GAROTTA, R., *Observation of shear waves and correlation with P events.* In *Seismic Shear Waves, Part B: Applications* (ed. G. Dohr) (Geophysical Press, London–Amsterdam 1985) pp. 1–86.

HASTINGS, D. S., *Cretaceous stratigraphy and reservoir potential, mid-Norway continental shelf.* In *Habitat of Hydrocarbons of the Norwegian Continental Shelf* (ed. A. M. Spencer *et al.*) (Graham and Trotman, London 1986) pp. 287–298.

HINZ, K., DOSTMAN, H. J., and HANISCH, J. (1984), *Structural Elements of the Norwegian Sea Continental Margin*, Geol. Jb. *A75*, 193–211.

LARSEN, B. T., KRIGSVOLL, R., and HEUM, O. R. (1989), *Structural style and tectonic development of the Haltenbanken area, Mid-Norway* (abstract), Norwegian Petrol. Soc. Conf. *Structural and Tectonic Modelling and its Application to Petroleum Geology* (Stavanger, 18–20 October 1989).

LARSEN, V. B. (1987), *A synthesis of Tectonically-related Stratigraphy in the North Atlantic-Arctic Region from Aalenian to Cenomanian Time*, Norsk Geologisk Tidsskrift *67*, 281–293.

MJELDE, R., BERG, E. W., STRØM, A., RIISE, O., SHIMAMURA, H., KANAZAWA, T., KODAIRA, S., and FJELLANGER, J. P. (1996), *An Extensive Ocean Bottom Seismograph Survey in the Vøring Basin, N. Norway*, First Break (in press).

MJELDE, R., and SELLEVOLL, M. A. (1993), *Seismic Anisotropy Inferred from Wide-angle Reflections off Lofoten, Norway, Indicative of Shear-aligned Minerals in the Upper Mantle*, Tectonophys. *222*, 21–34.

MUTTER, J. C. (1984), *Cenozoic and Late Mesozoic Stratigraphy and Subsidence History of the Norwegian Margin*, Bull. Geol. Soc. Am. *95*, 1135–1149.

PICETT, G. R. (1963), *Acoustic Character Logs and their Application in Formation Evaluation*, J. Pet. Tech. 659–667.

PLANKE, S., SKOGSEID, J., and ELDHOLM, O. (1991), *Crustal Structure off Norway, 62–70°N*, Tectonophys. *189*, 91–107.

RØNNEVIK, H. C., EGGEN, S., and VOLLSET, J., *Exploration of the Norwegian Shelf.* In *Petroleum Geochemistry and Exploration of Europe* (ed. J. Brooks) (Blackwell Scientific Publications, Oxford 1983) pp. 71–94.

SCHOENBERG, M., and PROTÁZIO, J. (1992), *"Zoeppritz" Rationalized and Generalized to Anisotropy*, J. Seismic Expl. *1*, 125–144.

SKOGSEID, J., and ELDHOLM, O., *Vøring Plateau Continental Margin: Seismic interpretation, stratigraphy and vertical movements.* In *Proc. ODP, Sci. Res. 104* (College Station, TX 1989) (Ocean Drilling Program) pp. 993–1030.

SKOGSEID, J., PEDERSEN, T., and LARSEN, V. B., *Vøring Basin: Subsidence and tectonic evolution.* In *Structural and Tectonic Modelling and its Application to Petroleum Geology* (ed. R. M. Larsen *et al.*) (NPF Special Publication *1*, Elsevier 1992) pp. 52–82.

SPENCER, A. M., *Petroleum Geology of the North European Margin* (Graham and Trotman, London 1984).

SPENCER, A. M., *Habitat of Hydrocarbons on the Norwegian Continental Shelf* (Graham and Trotman, London 1986).

SURLYK, F., PIASECKI, S., ROLLE, F., STEMMERIK, L., THOMSEN, E., and WRANG, P., *The Permian basin of East Greenland.* In *Petroleum Geology of the North European Margin* (ed. A. M. Spencer *et al.*) (Graham and Trotman, London 1984) pp. 303–315.

TALWANI, M., and UDINTSEV, G. *et al.* (1976), *Tectonic synthesis.* In *Initial Reports 38 (1976), Deep Sea Drilling Project*, pp. 1213–1242.

TATHAM, R. H., *Shear waves and lithology.* In *Seismic Shear Waves, Part B: Applications* (ed. G. Dohr) (Geophysical Press, London-Amsterdam 1985) pp. 86–133.

TATHAM, R. H., and MCCORMAC, M. D., *Rock physics measurements.* In *Multicomponent Seismology in Petroleum Exploration* (eds. E. B. Neitzel and D. F. Winterstein) (SEG Investigation in Geophysics Series *6*, 1991) pp. 43–91.

(Received November 18, 1995, accepted April 3, 1996)